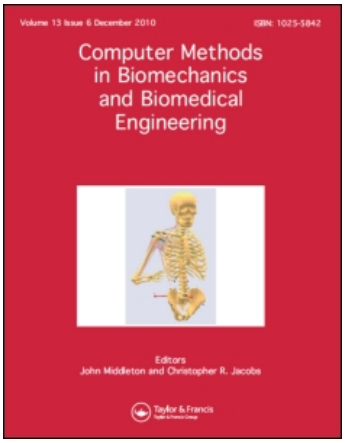

Computer Methods in Biomechanics and Biomedical Engineering
Publication details, including instructions for authors and subscription information:
http://www.informaworld.com/smpp/title~content=t713455284

Optimal mechanical design of anatomical post-systems for endodontic restoration

Franco Maceri[a]; Marco Martignoni[b]; Giuseppe Vairo[a]
[a] Dipartimento di Ingegneria Civile, Università di Roma 'Tor Vergata', Rome, Italy [b] Martignoni Associates, Rome, Italy

To cite this Article Maceri, Franco , Martignoni, Marco and Vairo, Giuseppe(2009) 'Optimal mechanical design of anatomical post-systems for endodontic restoration', Computer Methods in Biomechanics and Biomedical Engineering, 12: 1, 59 — 71
To link to this Article: DOI: 10.1080/10255840802164079
URL: http://dx.doi.org/10.1080/10255840802164079

Computer Methods in Biomechanics and Biomedical Engineering
Vol. 12, No. 1, February 2009, 59–71

Taylor & Francis
Taylor & Francis Group

Optimal mechanical design of anatomical post-systems for endodontic restoration

Franco Maceri[a], Marco Martignoni[b] and Giuseppe Vairo[a,*]

[a]*Dipartimento di Ingegneria Civile, Università di Roma 'Tor Vergata', Viale Politecnico 1, 00133 Rome, Italy;*
[b]*Martignoni Associates, Via M. Adelaide 6, 00196 Rome, Italy*

(*Received 4 August 2006; final version received 4 April 2008*)

This paper analyses the mechanical behaviour of a new reinforced anatomical post-systems (RAPS) for endodontic restoration. The composite restorative material (CRM) completely fills the root canal (as do the commonly used cast metal posts) and multiple prefabricated composite posts (PCPs) are employed as reinforcements. Numerical simulations based on 3D linearly elastic finite element models under parafunctional loads were performed in order to investigate the influence of the stiffness of the CRM and of the number of PCPs. Periodontal ligament effects were taken into account using a discretised anisotropic nonlinearly elastic spring system, and the full discrete model was validated by comparing the resulting stress fields with those obtained with conventional restorations (cast gold-alloy post, homogeneous anatomical post and cemented single PCP) and with the natural tooth. Analysis of the results shows that stresses at the cervical/middle region decrease as CRM stiffness increases and, for large and irregular root cavities that apical stress peaks disappear when multiple PCPs are used. Accordingly, from a mechanical point of view, an optimal RAPS will use multiple PCPs when CRM stiffness is equal to or at most twice that of the dentin. This restorative solution minimises stress differences with respect to the natural tooth, mechanical inhomogeneities, stress concentrations on healthy tissues, volumes subject to shrinkage phenomena, fatigue effects and risks of both root fracture and adhesive/cohesive interfacial failure.

Keywords: dental restorative material; finite element analysis; prefabricated composite post; post-endodontic restoration; anatomical post-systems; periodontal-ligament discrete model

1. Introduction

The physical and mechanical behaviour of materials for dental restoration never perfectly matches that of natural tissues. Consequently, the biomechanical balance of an endodontically treated tooth is different from that of a healthy tooth, and there may arise both stress concentrations and localised damages that can lead to restoration failure or to irreversible root fracture. Moreover, polymerisation of dental composite materials can produce shrinkage phenomena, ranging from 1.5 to 6% of the total volume (Davidson and de Gee 1984; De Gee et al. 1993; Davidson and Feilzer 1997; Labella et al. 1999), which may induce adhesive/cohesive imperfections and self-equilibrated stress fields (Hübsch et al. 2000; Barink et al. 2003; Versluis et al. 2004; Kleverlaan and Feilzer, 2005) that increase the risk of interfacial failure as well as post-operative sensitivity and recurrent caries (Brännström 1984; Eick and Welch 1986). Cyclic and thermal loading can act in synergy to amplify such effects (Lee et al. 2000, 2001) and can initiate a multistage failure process involving creation of interfacial micro-cracks, expansion and coalescence of macroscopic flaws into dominant cracks, and stable propagation of the dominant macro-cracks, according to the combination of opening, tear and shear modes occurring in multiaxial stress states.

The above-cited risks decrease when the number of different materials involved, stiffness discontinuities and material volumes subject to shrinkage are minimised.

Nowadays, in order to rehabilitate root canals and provide crown retention, restoration of pulpless teeth is usually performed using a post-reinforced structure based on prefabricated composite posts (PCPs), which are commercially available in different materials, geometries and dimensions. A post-and-core system is generally built up by cementing a fibre-reinforced PCP into the treated root cavity and embedding its out-of-root part into a composite resin core that supports the prosthetic crown.

Restoration based on PCP systems does not require great preparatory work, but the restoration can be critical when the treated root cavity is large and irregular. In this case, since the gap between the post and residual dentin has to be filled with a large amount of cement, significant shrinkage phenomena can arise. Furthermore, considerable discontinuities in material properties are introduced and the inevitable large interface between cement and composite core build-up can jeopardise the effectiveness and durability of the restoration.

For these reasons, anatomical posts (i.e. post-devices 'customised' to the profile of the treated root cavity) would appear to be more suitable than cylindrical endodontic

*Corresponding author. Email: vairo@ing.uniroma2.it

ISSN 1025-5842 print/ISSN 1476-8259 online

DOI: 10.1080/10255840802164079
http://www.informaworld.com

PCPs. It follows that cast-metal post-and-core systems (e.g., gold-alloy posts) fabricated from a mould taken directly from the root cavity (Baraban 1967) should be preferred, since they can provide close, smooth contact between the residual dentin and the restorative system. However, cast-metal posts require much preparatory work and can cause root fracture, since great inhomogeneity between the stiffnesses of the metal post and the dentin, possible contact imperfections and frictioning during material setting can introduce significant eigenstresses into the residual healthy structure. Accordingly, composite anatomical post-systems (APS) – customised posts made of a composite restorative material (CRM) with elastic properties similar to those of the natural tooth – should be the best solution. With respect to traditional cemented single-PCP systems (CSP), APSs have the advantage of eliminating the interface between filling cement and core resin, but they can suffer critical polymerisation shrinkage when the endodontic treatment produces a wide root cavity.

In order to overcome these drawbacks and preserve the advantages of APSs, we propose a reinforced anatomical post system (RAPS); that is, an APS equipped with multiple PCPs. This system can minimise shrinkage effects when the overall volume of the reinforcing PCPs increases and can reduce post pull-out risk. Longer restoration durability to fatigue can also be expected. As preliminarily proven in (Bisegna et al. 2003; Maceri et al. 2007) and as the proposed numerical results show, use of multiple PCPs increases the bearing capacity of the restored tooth, reduces stress peaks at the apex and thus eliminates the risk of irreversible apical fractures. Moreover, overstresses at the PCP interfaces disappear when the stiffness of the reinforcing post is of the same order of magnitude as that of the dentin. Accordingly, in this work we consider RAPSs equipped with glass-fibre PCPs of the same type proposed in (Pegoretti et al. 2002), based on an acrylic resin matrix [whose main component is bisphenol A glycidyl methacrylate (Craig 1989)], reinforced with unidirectional continuous *E*-glass fibres (Hybon 2001 by PPG Industries) with an average volume fraction of about 60%.

Recently, the use of APSs has been recommended by many clinicians (Fernandes et al. 2003) despite the lack of systematic investigation into the mechanical performance of this restorative technique. Dental literature has dedicated much space to cast post-systems and PCPs, analysing the influence of their geometries and materials on restored-tooth behaviour (e.g., Ko et al. 1992; Ho et al. 1994; Freedman 1996; Holmes et al. 1996; Kahn et al. 1996; Karna 1996; Sidoli et al. 1997; Martinez-Insua et al. 1998; Yaman et al. 1998; Asmussen et al. 1999; Pegoretti et al. 2002; Lanza et al. 2005). A numerical assessment of an APS without any reinforcing device was proposed by Genovese et al. (2005), but to our knowledge, quantitative results determining the influence of CRM and supporting its optimal choice for APSs and RAPSs are lacking.

Many researchers confirm that numerical simulation based on the finite element method can be an effective tool for evaluating the performance of restored teeth. A number of authors (e.g., Farah et al. 1973; Ko et al. 1992; Ho et al. 1994; Holmes et al. 1996; Silver-Thorn and Joyce, 1999; Ukon et al. 2000; Pegoretti et al. 2002; Toparli, 2003) propose two-dimensional (2D) dental models in which plane strain behaviour is assumed. Clearly, 2D models are easy to implement and save computing time, but results in these cases can be unrealistic in terms of both stresses and strains (Romeed et al. 2006). Experimental tests, photo-elastic analyses and clinical observations, instead, prove three-dimensional (3D) models to be more suitable and accurate for describing the real mechanical behaviour of the restored tooth (e.g., Yaman et al. 1998; Joshi et al. 2001; Hubsch et al. 2002; Pierrisnard et al. 2002; Versluis et al. 2004; Asmussen et al. 2005; Genovese et al. 2005; Lanza et al. 2005; Ichim et al. 2006).

In this paper, the influence of the stiffness of the CRM on the mechanical performance of a lower premolar restored through the RAPS technique is analysed by means of static 3D linearly elastic finite element models. An anisotropic nonlinear elastic model of the periodontal ligament (PDL) is used to suitably describe tooth/bone interaction effects. RAPSs equipped with one or three PCPs are investigated under several parafunctional loads. Comparisons of the resulting stress fields with those obtained with conventional cast gold alloy and APS restorations and with those of the natural tooth highlight the great importance of the elastic properties of the CRM in successful restoration.

2. Materials and methods

Our study refers to a human lower premolar, the 3D solid model of which was built up using a parametric cubic-interpolation algorithm. It was implemented in a home-made MATLAB® code, which uses pictures or X-ray images and some prescribed morphological/clinical parameters to reproduce the geometries of endodontically treated teeth (Vairo 2003).

With reference to Figure 1, the following models were built up and analysed:

- pulpless tooth restored using a cemented single-PCP (CSP);
- pulpless tooth restored using a cast gold-alloy post (CGP);
- pulpless tooth restored using a composite anatomical system (APS);
- pulpless tooth restored using reinforced anatomical systems, equipped with one ($RAPS_1$) or three ($RAPS_3$) reinforcing PCPs (conic 2%);
- natural tooth (NT).

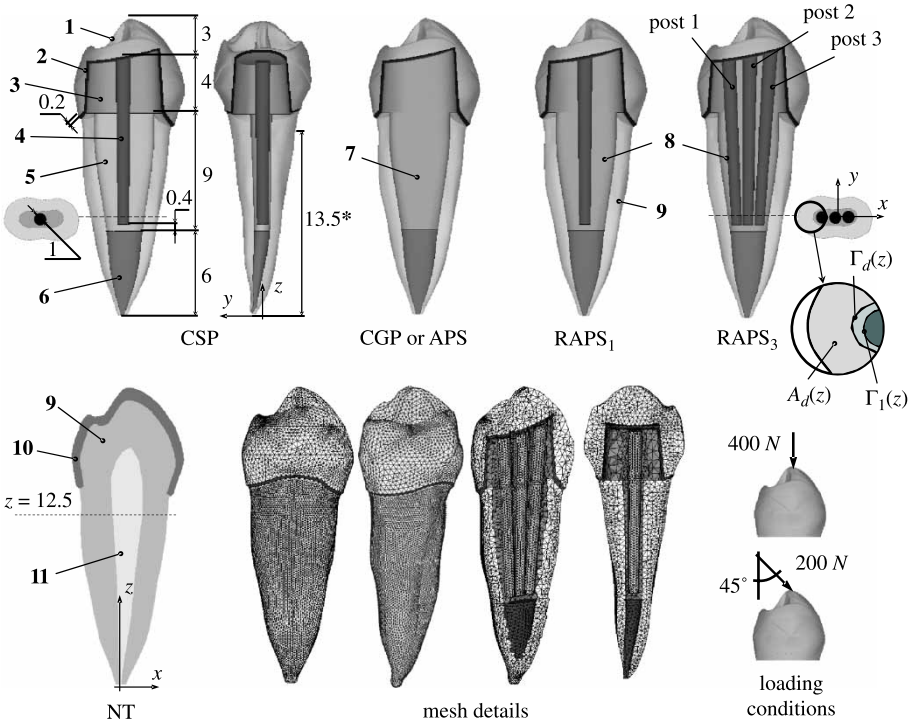

Figure 1. Geometries, intervention regions, notations, loading conditions and some mesh details. 1, Restored crown; 2, crown-core adhesive layer; 3, composite core build-up; 4, prefabricated composite post (conic 2%); 5, filling cement; 6, guttapercha; 7, cast gold-alloy post or composite anatomical system; 8, reinforced anatomical post; 9, dentin; 10, enamel and 11, pulp. Dimensions in mm (symbol '*' identifies the PDL region).

Each restoration was considered in its definitive configuration; i.e. with a prosthetic ceramic crown linked to the core build-up by an adhesive layer. Moreover, in order to make significant comparisons, the thickness of the residual dentin was assumed to be the same in all the restored-tooth models analysed.

In order to investigate limit conditions related to biting or chewing of very tough foods (Howell and Manly 1948; Anderson 1956) and to bruxism (Nishigawa et al. 2001), two static loads were considered separately. The first consisted in a vertical intrusive force of 400 N applied at the top of the crown; the second, an oblique force (angled at 45° with respect to the occlusal plane) of 200 N applied at the same point and oriented towards the labial side.

The commercial finite element tool ANSYS® 7.1 was used to implement and discretise the solid models. Three-dimensional meshes, based on quadratic 10-node tetrahedral elements with three degrees of freedom per node, were generated. On the basis of convergence analysis results, an average mesh-size of about 0.2 mm was chosen. The restored-tooth models include about 130,000 elements and 185,000 nodes. Continuity of displacement fields through material interfaces was enforced; that is, perfect bonding between different materials was assumed. Models, some details of finite-element meshes, loading conditions and relevant notations are shown in Figure 1. Note that the anatomical systems (both APSs and RAPSs) do not have any material interface separating the core from the filling region.

Dry-material models (i.e. models disregarding any fluid–solid interaction) were employed and dynamic and viscous effects were likewise ignored. All constitutive parts of the (restored) tooth were taken as being homogeneous and all materials were modelled as linearly elastic and isotropic, to the exception of the PCPs, which were considered as being transversally isotropic. Table 1 summarises the relevant elastic constants. For sensitivity analysis of the performance of the APSs and RAPs, both commercial and ideal CRMs were investigated, varying the Young's modulus of the CRM. In the case of the conventional CSP system, Relix Unicem (3M ESPE AG, Seefeld, Germany) and Clearfil F2 (Kuraray, Osaka, Japan) were considered as filling cement and core resin, respectively.

Finite-element models are constrained by a nonlinear discrete spring system modelling the PDL. As proposed in Maceri et al. (2007), PDL response to compression, tension and shear is locally fitted through 3D springs connecting nodes on the root's outer boundary (see Figure 1) to the cortical bone. Due to its high stiffness, the bone is assumed to be a rigid, fixed body. For each dentinal-PDL node,

Table 1. Elastic constants adopted for FE analyses. E and G indicate the Young's and shear modulus, respectively (tangent moduli), whereas ν is the Poisson's ratio. Referring to PCPs, the quantities in square brackets indicate properties evaluated in transverse-to-fibre direction.

Material	E (GPa)	ν	G (GPa)
Dentin[a,b]	18.6	0.31	
Enamel[a,b]	41.0	0.30	
Pulp[c]	0.98×10^{-3}	0.45	
Restored crown (ceramic)[d]	380.0	0.25	
Adhesive layer crown-core[e]	7.6	0.30	
Cast metal post (ILOR56: gold-alloy)[b]	93.0	0.33	
Glass-fibre PCPs[b]	40.0 [11.0]	0.26 [0.32]	4.2 [4.1]
Guttapercha[a,b]	0.69×10^{-3}	0.45	
Restorative materials:			
Relix Unicem[e] (RU)	5.6	0.33	
Clearfil F2[f] (CF)	12.4	0.30	
Build-It FR[g] (BI)	15.5	0.30	
Ideal material 1 (IM1)	18.6	0.30	
Ideal material 2 (IM2)	30.0	0.30	
Ideal material 3 (IM3)	100.0	0.30	

[a] From Ko et al. (1992).
[b] From Pegoretti et al. (2002).
[c] From Genovese et al. (2005).
[d] Alumina ceramic Procera; data provided by the manufacturer (Nobel Biocare, Gothenborg, Sweden).
[e] Variolink II + Heliobond; data provided by the manufacturer (Ivoclar Vivadent, Schaan, Liechtenstein).
[f] Relix Unicem; data provided by the manufacturer (3M ESPE AG, Seefeld, Germany).
[g] Clearfil F2; data provided by the manufacturer (Kuraray, Osaka, Japan).

a spring-chain of eight linearly elastic elements was introduced; each spring element acts in both the normal-to-dentin and parallel-to-dentin directions, in given elongation intervals. Stiffness depends on the transverse shear and Young moduli as well as on the local thickness of the PDL, which is assumed to be quadratically variable along the root axis (Figure 2b), in accordance with least-squares fitting of the experimental data proposed by Toms et al. (2002).

The spring-model stiffnesses in the normal-to-dentin direction were calculated by the tangent Young's modulus of the PDL, which is computed (Figure 2a) as the slope of a piecewise linear least-squares fitting Maceri et al. (2007) of the stress/strain experimental curve proposed by Nishihira et al. (2003) in the case of a quasi-static deformation-rate response (0.005% per second). As the authors demonstrated in Maceri et al. (2007), investigation of the bearing capacity of the restored structure using an elastic constraint model based on the quasi-static PDL response results, is more conservative, from an engineering point of view, than is a method based on the PDL's short-term-loading behaviour.

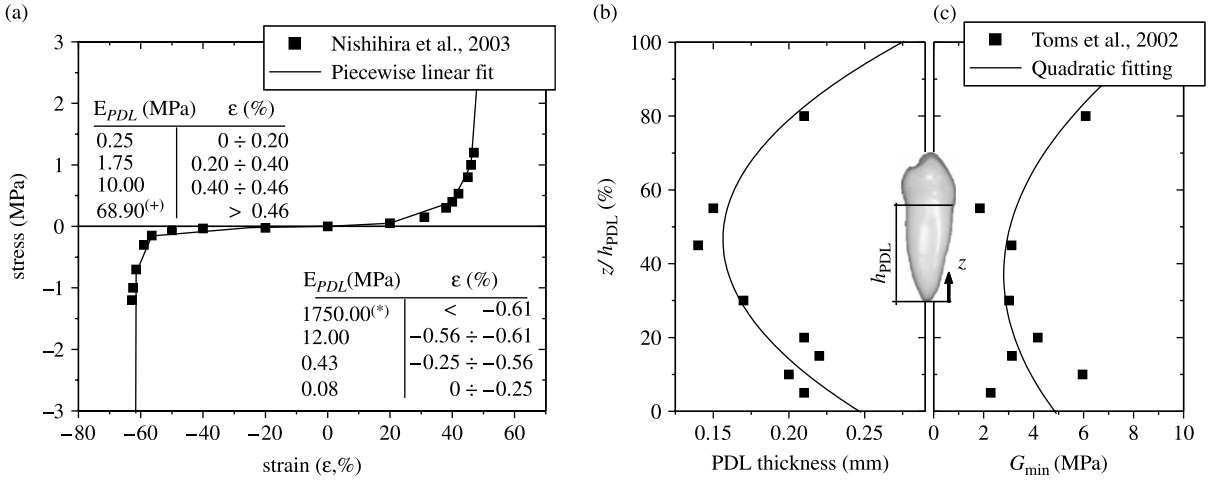

Figure 2. Nonlinear model of the periodontal ligament. Experimental data and fitting results used for numerical model setting ((+) from Ko et al. (1992); (*) from Goel et al. (1992)).

Parallel-to-dentin stiffnesses are computed by assuming that shear reactions appear whenever the local shear strain γ exceeds 0.25 rad, in accordance with the average behaviour observed in Toms et al. (2002). Let $G_{\min}(z)$ be the value of the transverse modulus obtained (Figure 2c) by quadratic least-squares fitting Maceri et al. (2007) of the experimental data proposed by Toms et al. (2002) for pure shear tests (i.e. when $\varepsilon = 0$, ε being the PDL's strain along the direction at right angles to the tooth's surface), and let $G(\varepsilon)$ be the transverse modulus obtained by assuming PDL to be a nearly incompressible isotropic material [i.e. with Poisson's ratio equal to 0.45 (Pegoretti et al. 2002)] whose Young's modulus at the actual ε is given by the above cited piecewise linear fitting. Accordingly, when $\gamma > 0.25$ rad, local shear stiffnesses are established by assuming the value of the actual transverse elastic modulus $G_{\mathrm{PDL}}(\gamma, \varepsilon, z)$ to be equal to the maximum between $G_{\min}(z)$ and $G(\varepsilon)$.

The PDL spring elements were generated and added to the finite element models using a homemade Fortran preprocessing code, taking as input the primary topological data (i.e. nodal coordinates and elements lying on the PDL region). Due to the nonlinearity of the PDL model, the nonlinear numerical analyses must consider a large displacement finite-element formulation. The iterative procedure employs a modified Newton–Raphson approach based on the arc-length method (Zienkiewicz and Taylor 1998).

Analysis of the numerical results was carried out in consideration of some risk indicators relevant to root fracture and adhesive/cohesive interfacial failure, based on well-known stress measures: Von Mises equivalent stress σ_{VM}, Rankine equivalent stress σ_{R} and shear stress modulus τ_{n} (Drucker 1967).

The Von Mises stress field, which gives a measure of the average stress level, is widely cited in dental literature (e.g., Farah et al. 1973; Ko et al. 1992; Ho et al. 1994; Holmes et al. 1996; Yaman et al. 1998; Silver-Thorn and Joyce 1999; Ukon et al. 2000; Joshi et al. 2001; Pierrisnard et al. 2002; Pegoretti et al. 2002; Toparli 2003; Versluis et al. 2004; Genovese et al. 2005; Lanza et al. 2005; Asmussen et al. 2005; Ichim et al. 2006; Romeed et al. 2006). Starting from the field σ_{VM}, the mean Von Mises stress $\sigma^*_{\mathrm{VM}}(z)$ risk indicator is introduced as a function of the z-coordinate along the tooth's axis. This function is calculated for the residual dentin and, with reference to the notations introduced in Figure 1, is given by the average of σ_{VM} on the 2D region $A_{\mathrm{d}}(z)$; i.e. on the dentinal cross-section area at the root level z.

In order to investigate the risk of fragile root fracture and interfacial cohesive failure, we also considered Rankine equivalent stresses σ_{R}, for both the tensile state (index t) and the compressive state (index c).

With reference to Figure 1, let $\Gamma_{\mathrm{d}}(z)$ be the 2D curve obtained by intersecting a plane orthogonal to the z-axis with the 3D interface between the CRM region and the residual dentin. Analogously, let $\Gamma_{\mathrm{i}}(z)$ be the 2D CRM interface with the ith PCP. Tensile and compressive Rankine stress fields are used in computing the functions $\sigma^*_{\mathrm{Rt}}(z)$ and $\sigma^*_{\mathrm{Rc}}(z)$ at both the residual dentin interface [i.e. considering $A_{\mathrm{d}}(z)$] and the CRM interface [i.e. considering $\Gamma_{\mathrm{d}}(z)$ or $\Gamma_{\mathrm{i}}(z)$]. These functions are calculated taking the maximum and the minimum of the fields σ_{Rt} and σ_{Rc}, respectively, in a given domain ($A_{\mathrm{d}}(z)$ or $\Gamma_{\cdot}(z)$). Accordingly, $\sigma^*_{\mathrm{Rt}}(z)$ and $\sigma^*_{\mathrm{Rc}}(z)$ can be considered as being risk indicators of fragile root fracture (if referred to residual dentin) and of local cohesive failure (for CRM interfaces).

Finally, field τ_{n} is computed at the generic point of a given interfacial surface as the modulus of the relevant shear stress. This field is used to calculate the function $\tau^*_{\mathrm{n}}(z)$, defined as the maximum value of τ_{n} on a given interfacial curve $\Gamma_{\cdot}(z)$. Since high interfacial shear stresses can lead to detachment of concurrent materials, function $\tau^*_{\mathrm{n}}(z)$ gives a measure of the interfacial adhesive failure risk.

3. Results and discussion

Figures 3 and 4 show Von Mises stresses on the tooth cross-section at $y = 0$ for vertical and oblique loads, respectively. Figure 5 illustrates the mean Von Mises stress function $\sigma^*_{\mathrm{VM}}(z)$, and Figure 6 shows σ_{VM} path-plots along the line $\{y = 0, z = 12.5\}$ defined in Figure 1. Composite anatomical restorations, both with and without glass-fibre reinforcements (RAPS and APS, respectively) are compared with traditional restorations (cemented PCP and cast gold-alloy post) as well as with the natural tooth.

Composite anatomical restorations (APSs) show more homogeneous Von Mises stress distributions than do conventional cemented single-post (CSP) and cast-metal post (CGP) restorations. It is worth observing that, when the CRM's stiffness is comparable to the dentin's, stress fields are smooth and uniform and, at dentinal region, are very similar to the natural tooth's. If BI and IM1 (see Table 1 for notations) are used as CRMs, the natural tooth's behaviour at the middle root level is practically reproduced and stress peaks at the cervical margins are significantly lower than those of the CSP. Analysis of Figure 5 highlights that, for RAPSs, dentinal mean stresses decrease in the cervical/middle regions when the CRM Young's modulus (E_{CRM}) and/or the number of PCPs increase, the first effect being dominant for high-stiffness CRMs. In detail, for RAPS_3 restorations based on BI and IM1 ($E_{\mathrm{CRM}} = 18$–30 GPa), mean stress peaks at cervical margins are, with respect to the CSP restoration, about 24% lower for vertical load and 13% lower for oblique load. Moreover, as Figures 3, 4 and 6 show, average stresses are decreasing functions of CRM stiffness but there can also exist high stress gradients at dentin/post-system interfaces, as in the case of CGP restorations. As has been previously remarked, this is a serious drawback of cast metal post-systems, since possible

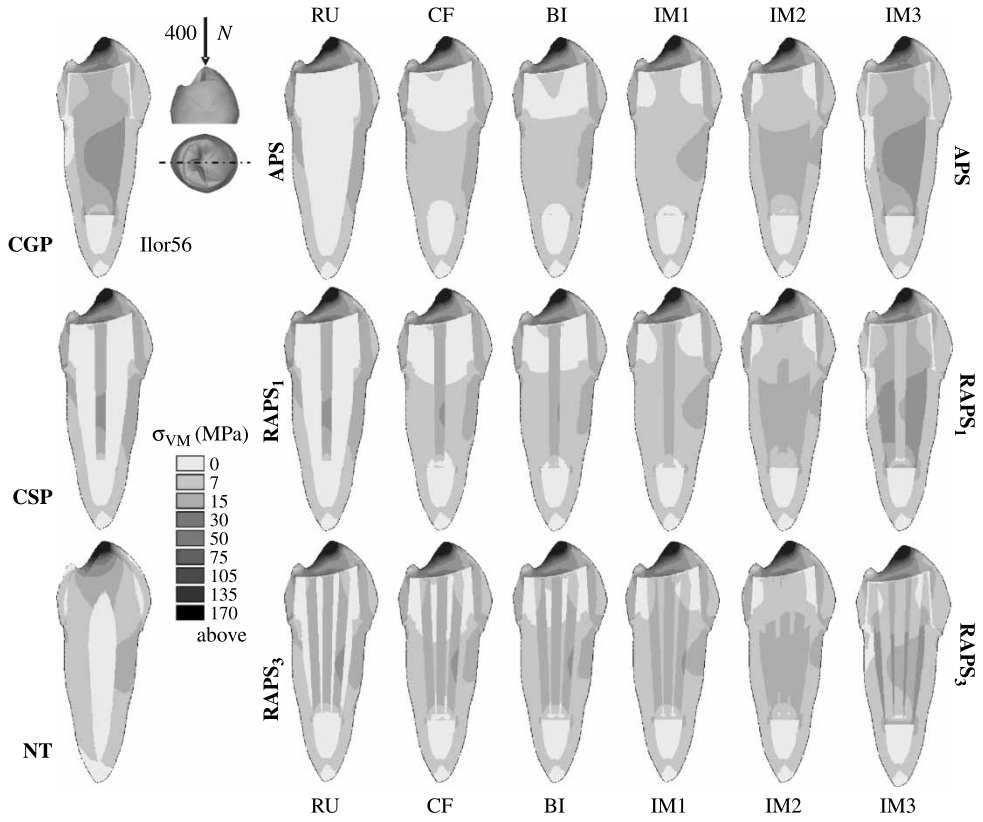

Figure 3. Von Mises stress contours on the tooth cross-section at $y = 0$. Comparison between different models for vertical intrusive load.

contact inhomogeneities and setting imperfections may lead to local dentinal overstresses. Nevertheless, in the case of IM3 ($E_{CRM} = 100$ GPa) these troubles could be reduced if suitable filling and polymerisation procedures were to be developed.

Analysis of Figure 5 also shows that, with respect to the behaviour of the natural tooth and whatever the CRM stiffness value, great stress concentrations appear at the root apex with CGP-, CSP-, APS- and $RAPS_1$-restorations.

On the contrary, in case of $RAPS_3$ restorations (i.e. APS equipped with three glass-fibre PCPs), we see a significant reduction of the apical stresses that does not seem to depend on the composite restorative material. Nevertheless, Figures 3, 4 and 6 prove that stress gradients at the PCP/CRM interfaces increase when E_{CRM} is very different from E_{PCP} (i.e. from the Young's modulus of PCPs).

Figure 7 illustrates the Rankine stress functions $\sigma^*_{Rt}(z)$ and $\sigma^*_{Rc}(z)$ calculated at the residual healthy tissue region for investigation of root-fracture risk. Diagrams relevant to the material IM2 only are showed, whereas maximum values of $\sigma^*_{Rt}(z)$ and $|\sigma^*_{Rc}(z)|$, evaluated also for the other cases at different regions of the residual dentin, are summarised in Table 2. It is clear that, with respect to the CSP solution and for both compressive and tensile states, root-fracture risk at the cervical margins declines when the stiffness of the CRM increases. For instance, use of BI gives the following reductions: about 10% for APS and 13% for $RAPS_3$ under intrusive load; about 7–9% for APS, and about 10–15% for $RAPS_3$ under oblique load. With IM2: about 19% for APS and 21% for $RAPS_3$, under intrusive load; 10–17% for APS and 12–18% for $RAPS_3$, under oblique load.

Moreover, whatever the CRM stiffness value and with respect to CSP, APS and CGP, apical root-fracture risk drastically diminishes (by about 15–30% for vertical load and 30–40% for oblique load) with $RAPS_3$ treatment. It is worth observing that a single central reinforcing PCP ($RAPS_1$ case) does not cause any reduction of the apical stresses. Furthermore, although for $RAPS_3$ restorations based on IM3 the stiffness of the PCPs is much lower than the CRM's (see Table 1), distribution of glass-fibre posts in the root cavity far from the tooth's axis permits reducing the apical stress level in any case. Hence, for IM3-based $RAPS_3$ restorations, stresses are everywhere lower than in APS and $RAPS_1$ cases.

As far as the CRM's interfaces are concerned, Figure 8 illustrates functions $\tau^*_n(z)$, $\sigma^*_{Rt}(z)$ and $\sigma^*_{Rc}(z)$ at the reinforcing PCP interfaces (for RAPS models), whereas Table 3 summarises the failure-risk indicators at the root

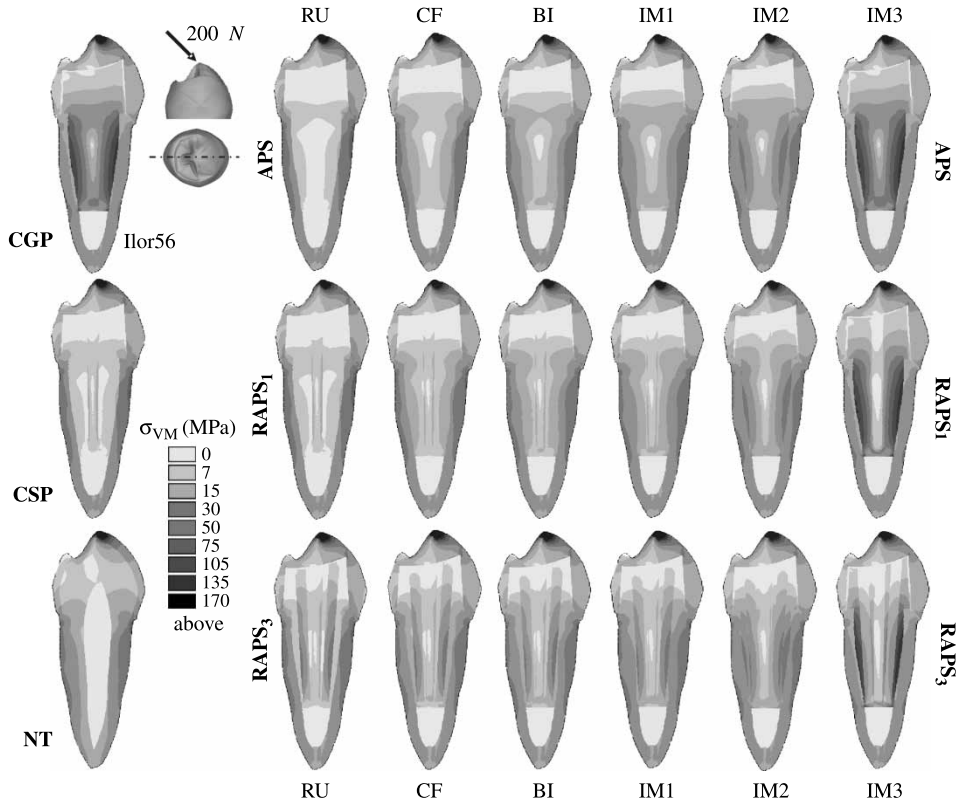

Figure 4. Von Mises stress contours on the tooth cross-section at $y = 0$. Comparison between different models for oblique intrusive load.

cavity interface in both APS and RAPS solutions. The resulting interfacial stresses, evaluated considering different CRM-stiffness values, are compared with the stresses for CSP solution. It is worth to note that Figure 8 refers, for the case $RAPS_3$, only to the central post (i.e. post 2 in Figure 1). Similar results, in both a qualitative and quantitative sense, were numerically experienced for lateral reinforcing posts.

In the case of cemented single-PCP treatment, the high shear stress gradients that appear at the filling-cement/core-resin interface (see Figure 8) can induce detachment processes. This effect completely disappears when that interface is suppressed; i.e. in anatomical restorations.

In these cases, analysis of interfacial shear stress shows also that adhesion could be critical at both the top and bottom levels of the filling region (both for CRM/dentin and PCP/CRM interfaces). On the other hand, mean shear stresses at CRM/dentin interfaces increase with E_{CRM} (Table 3) and they depend in large part on the difference in stiffness between the PCP and the CRM at the reinforcement interfaces (Figure 8).

Furthermore, interfacial Rankine stress functions are sufficiently smooth and uniform for all the CRMs investigated, and their values increase when the CRM's stiffness increases. Accordingly, the greatest cohesive failure risk appears in the case of IM3-based restorations, whereas Rankine stresses are acceptable for the other CRMs.

Previous results show that, with IM3, detachment can arise at the PCP interfaces (Figure 8) if the adhesive and cohesive limits are less than about 40 and 120 MPa, respectively. Analogously, as far as the root cavity interface is concerned (Table 3), critical adhesive and cohesive limits are about 80 and 160 MPa, respectively. These values decrease sharply when IM1 and IM2 are used, becoming practically comparable to the values obtained using commercially available materials. Nevertheless, we should not forget that the stress concentrations at the PCP interfaces are localised in the sharp edges of the glass-reinforcements; therefore, using smooth conical PCP ends could significantly reduce this drawback (see Pegoretti et al. 2002).

As a matter of fact, CRMs much stiffer than dentin can reduce stress on the residual healthy tissue but, at the same time, can increase interfacial stresses. In our opinion, a correct compromise with respect to these two

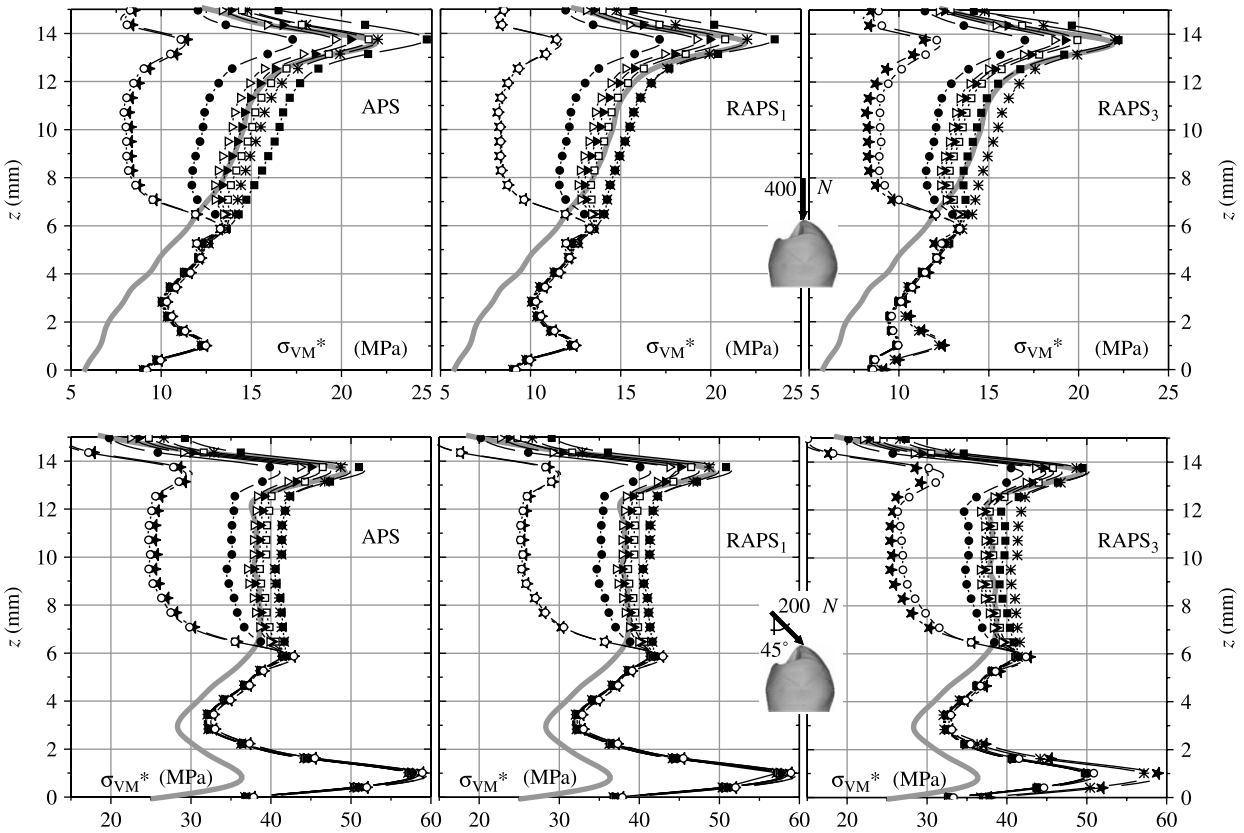

Figure 5. Mean Von Mises stress function $\sigma^*_{VM}(z)$ at the residual dentin. Comparisons between different models. —, Natural tooth; – ★ –, cast gold-alloy post; – * –, cemented single-PCP; – ■ –, composite restorative material (CRM): RU; – □ –, CRM: CF; – ▲ –, CRM: BI; – △ –, CRM: IM1; – • – CRM: IM2; – ◦ – CRM: IM3.

conflicting effects is represented by IM1 or IM2 composite restorative materials. The former is characterised by the same stiffness as dentin, whereas the Young's modulus of the latter is 30 GPa; i.e. about twice that of dentin.

4. Conclusions

This paper investigates the influence of the elastic properties of composite restorative material (CRM) on the mechanical performance of endodontic restorations based on anatomical post-systems reinforced by prefabricated composite posts (RAPS).

Analysis was carried out through a 3D finite-element approach, considering a static linear discrete model of a human lower premolar under different parafunctional loads. In order to take into account the nonlinear interaction effects between restored tooth and cortical bone, a discretised anisotropic nonlinearly elastic model of the periodontal ligament (PDL) was employed. RAPS model is discussed in comparison with other restoration techniques – i.e. cemented single-PCP (CSP), cast gold-alloy post (CGP), non-reinforced anatomical post (APS) – and the natural tooth.

Simulation results show that, with reference to the behaviour of the natural tooth, stress concentrations appear at the apical and cervical levels in conventional restorations and with low-stiffness APSs. Moreover, in the case of CGP, high stress gradients are experienced at the post-system/dentin interface. On the contrary, APSs based on a CRM whose stiffness is comparable to dentin's produce more uniform and smoother stress distributions and at the same time eliminate the CSP's critical interface between filling cement and core resin.

Comparisons with the CSP results show that APSs with $E_{CRM} = 12 - 100$ GPa (E_{CRM} being the Young's modulus of the CRM) induce a significant stress reduction into the residual healthy tissue at the cervical/middle root regions, whereas no effect appears on the apical tensional peaks (which arise in CSP, CGP and APS restorations).

On the other hand, when RAPSs are used, apical overstresses are greatly reduced, and in a way which clearly depends on the number of PCPs and not on the stiffness of the CRM. When a single central reinforcing PCP is considered ($RAPS_1$) no significant variation of the apical stresses appears, whereas they decrease sharply in the case of anatomical post-systems equipped with three glass-fibre PCPs ($RAPS_3$).

It is worth observing that multiple reinforcement also offers other significant advantages: volumes undergoing

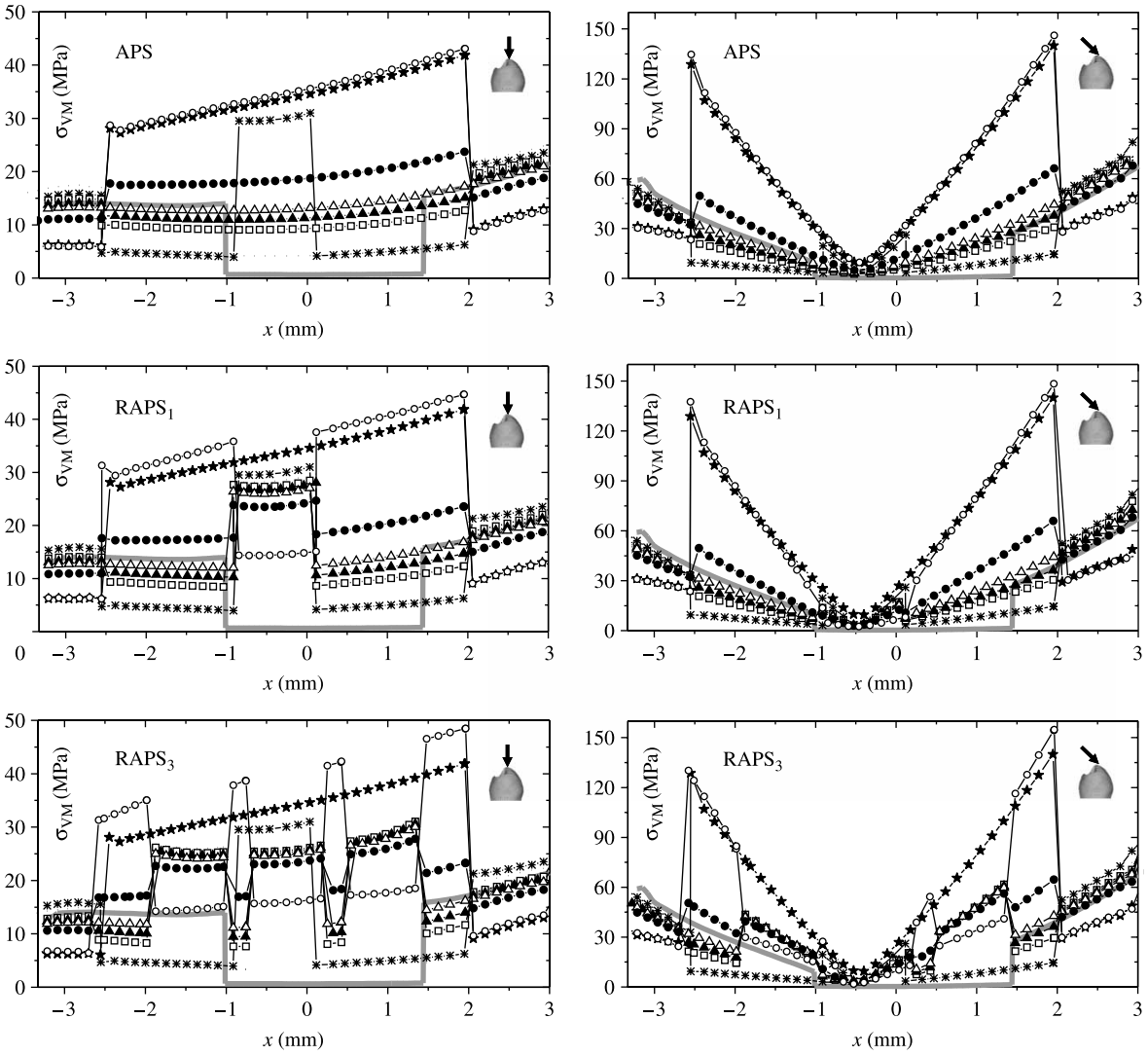

Figure 6. Path-plots along the line $\{y = 0, z = 12.5\}$ of Von Mises stress σ_{VM}. Comparisons between different models. The symbols are the same of Figure 5.

shrinkage effects are reduced and a larger overall core-post interface is obtained. Therefore, the post pull-out risk is reduced and a longer restoration durability to fatigue can be expected.

The proposed numerical results point up that the influence of CRM stiffness is significant at the middle/cervical levels, whereas multi-post treatment reduces apical and cervical stress peaks. In order to maximise both effects, in the sense of the dentinal stress reduction, a $RAPS_3$ restoration based on an ideal composite restorative material (IM3) with a stiffness value comparable to that of the gold alloy post (Ilor56) should be considered. Nevertheless, although contact inhomogeneities and setting imperfections (which may lead to local dentinal overstresses) could be ideally minimised through suitable filling and polymerisation procedures, in practice this solution could be delicate to handle because of the high induced stress gradients at the CRM/PCP and CRM/dentin interfaces.

Indeed, analysis of the failure-risk indicators at these interfaces (with respect both to adhesive and cohesive failure) shows that their maximum values increase when the restorative material's stiffness increases. Nevertheless, interfacial stresses are acceptable if E_{CRM} is of the same order of magnitude as the dentin's. In any case, stress concentrations at the PCP edges can be reduced by employing suitable geometric solutions such as smooth conical ends.

Finally, when the endodontic treatment leads to wide root cavities, the optimal mechanical behaviour for the restored structure is obtained with RAPS restorations

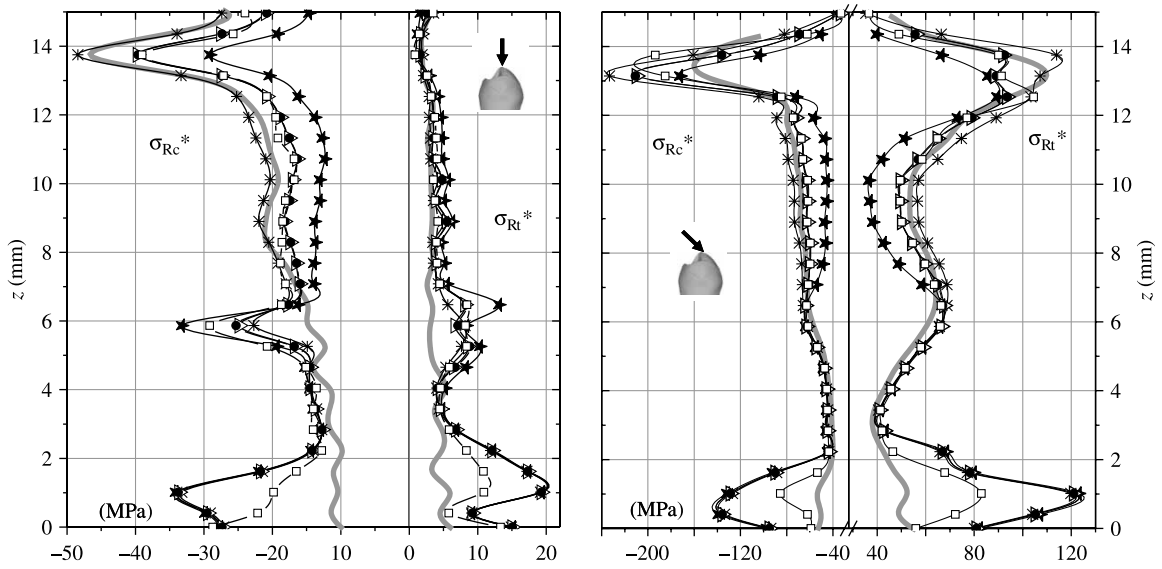

Figure 7. Rankine stress functions $\sigma^*_{Rt}(z)$ and $\sigma^*_{Rc}(z)$ at the residual dentin. Comparisons between different models. —, Natural tooth; – ★ –, cast gold-alloy post; – * –, cemented single-PCP; – △ –, IM2-based APS; – • –, IM2-based $RAPS_1$; – □ – IM2-based $RAPS_3$.

Table 2. Maximum values (in MPa) of Rankine stress functions σ^*_{Rt} ($|\sigma^*_{Rc}|$) at different regions of the residual dentin.

	Vertical load			Oblique load		
	Apical[a]	Middle[b]	Cervical[c]	Apical[a]	Middle[b]	Cervical[c]
NT	7.3 (11.7)	3.8 (21.0)	3.6 (46.4)	59.5 (55.5)	63.9 (68.6)	109.4 (153.3)
CGP	19.4 (34.1)	13.1 (33.2)	4.9 (29.1)	123.1 (139.0)	66.9 (63.4)	89.5 (172.1)
CSP	19.2 (33.2)	8.2 (22.7)	3.9 (49.4)	119.8 (133.8)	68.8 (74.3)	113.9 (235.3)
APS						
RU	19.2 (33.2)	5.6 (22.7)	4.6 (52.5)	119.9 (133.8)	66.8 (74.7)	116.5 (234.8)
CF	19.2 (33.4)	6.9 (21.3)	3.4 (47.1)	120.2 (134.3)	68.2 (70.9)	106.6 (226.2)
BI	19.2 (33.5)	7.2 (22.0)	3.2 (45.3)	120.3 (134.5)	67.9 (69.3)	103.3 (218.7)
IM1	19.2 (33.6)	7.6 (22.6)	3.2 (43.8)	120.4 (134.8)	67.7 (67.6)	100.4 (215.7)
IM2	19.3 (33.7)	8.5 (24.9)	3.5 (39.7)	121.1 (135.8)	67.4 (64.0)	93.2 (204.9)
IM3	19.4 (34.1)	13.3 (33.7)	5.0 (28.6)	123.3 (139.2)	66.7 (63.1)	89.3 (168.1)
$RAPS_1$						
RU	19.2 (33.3)	8.2 (22.7)	4.4 (50.9)	119.9 (133.8)	68.8 (74.4)	116.2 (234.1)
CF	19.2 (33.4)	8.1 (23.3)	3.4 (46.2)	120.2 (134.3)	68.1 (70.8)	106.7 (226.1)
BI	19.2 (33.6)	8.3 (23.6)	3.2 (44.6)	120.3 (134.6)	67.8 (69.3)	103.7 (223.1)
IM1	19.2 (33.5)	8.4 (23.8)	3.3 (43.3)	120.5 (134.8)	67.4 (67.9)	100.7 (220.2)
IM2	19.3 (33.8)	8.8 (25.3)	3.5 (39.6)	121.0 (135.8)	66.9 (63.6)	93.6 (210.5)
IM3	19.4 (34.1)	13.0 (33.2)	4.8 (29.1)	123.3 (139.3)	65.8 (62.2)	89.5 (171.3)
$RAPS_3$						
RU	13.3 (28.6)	8.1 (25.5)	5.2 (48.0)	82.1 (84.4)	67.5 (70.7)	109.5 (208.3)
CF	13.3 (28.7)	8.2 (27.2)	4.6 (44.2)	82.3 (84.8)	67.0 (67.8)	105.2 (203.1)
BI	13.3 (28.7)	8.2 (27.6)	4.3 (43.0)	82.5 (84.9)	66.8 (66.6)	104.5 (201.0)
IM1	13.3 (28.7)	8.2 (28.0)	4.1 (41.7)	82.6 (85.0)	66.7 (65.5)	103.6 (199.2)
IM2	13.2 (28.7)	8.4 (29.2)	4.1 (39.0)	83.0 (85.6)	66.3 (62.9)	102.5 (193.6)
IM3	13.2 (28.6)	15.3 (35.8)	4.8 (30.3)	84.4 (87.4)	65.9 (62.3)	100.4 (171.9)

[a] $z \in (0,4)$ mm.
[b] $z \in (4,10)$ mm.
[c] $z \in (10,15)$ mm (see Figure 1).

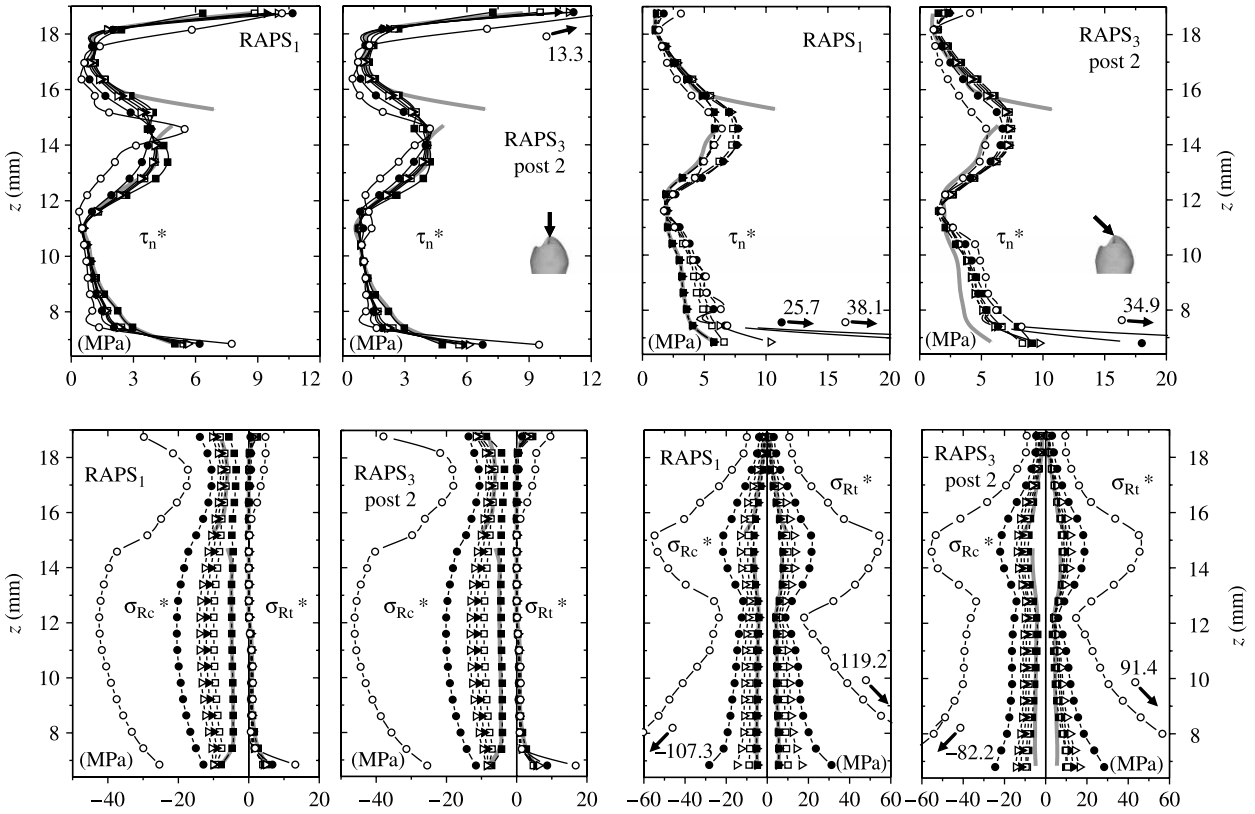

Figure 8. Shear and Rankine stress functions $\tau_n^*(z)$, $\sigma_{Rt}^*(z)$ and $\sigma_{Rc}^*(z)$ for CRM at the PCP interfaces. $RAPS_1$ and $RAPS_3$ restorations under vertical (left) and oblique (right) load. —, CSP; – ■ –, CRM: RU; – □ –, CRM: CF; – ▲ –, CRM: BI; – △ –, CRM: IM1; – • – CRM: IM2; – ◦ –, CRM: IM3.

Table 3. Adhesive and cohesive failure risk indicators at CRM/dentin interface. Mean ($\bar{\tau}_n^*$) and maximum ($\tau_{n\,max}^*$) values (in MPa) of shear stress function, and maximum values (in MPa) of Rankine stress functions σ_{Rt}^*, σ_{Rc}^*. Comparisons between cemented single-PCP and anatomical restorations (both APS and RAPS).

	Vertical load			Oblique load		
	APS	$RAPS_1$	$RAPS_3$	APS	$RAPS_1$	$RAPS_3$
	CSP: 3.3 (10.2)		$\bar{\tau}_n^*(\tau_{n\,max}^*)$	CSP: 7.3 (21.4)		
RU	2.7 (6.0)	3.2 (9.8)	3.3 (9.6)	6.7 (18.5)	6.8 (19.3)	6.9 (17.3)
CF	4.0 (9.7)	4.2 (12.0)	4.1 (11.8)	10.2 (37.1)	10.2 (36.5)	9.7 (34.1)
BI	4.4 (10.6)	4.5 (12.5)	4.4 (12.2)	11.5 (44.7)	11.4 (43.6)	10.7(41.6)
IM1	4.7 (11.3)	4.8 (12.9)	4.7 (12.4)	12.6 (51.9)	12.5 (50.2)	11.6 (48.6)
IM2	5.9 (13.3)	5.8 (13.5)	5.5 (12.6)	16.1 (75.9)	15.9 (72.9)	15.0 (72.2)
IM3	10.2 (39.6)	10.3 (41.3)	9.8 (42.8)	23.4 (85.2)	23.6 (84.1)	23.9 (86.4)
	CSP: 3.9 (11.1)		$\sigma_{Rt\,max}^*(\sigma_{Rc\,max}^*)$	CSP: 17.0 (17.4)		
RU	1.9 (8.1)	3.8 (7.3)	3.9 (10.3)	16.4 (17.8)	16.4 (17.7)	16.8 (17.0)
CF	3.1 (14.9)	3.9 (16.8)	4.3 (16.9)	31.6 (35.8)	31.6 (35.8)	30.6 (34.3)
BI	3.4 (17.4)	4.1 (19.0)	5.1 (18.0)	37.7 (43.2)	16.4 (17.7)	37.0 (41.6)
IM1	4.3 (19.8)	4.2 (21.1)	6.0 (19.9)	43.8 (50.2)	43.6 (50.2)	43.3 (48.5)
IM2	8.6 (27.1)	8.3 (27.7)	9.0 (25.9)	65.1 (72.9)	65.3 (73.0)	64.1 (71.7)
IM3	31.9 (63.3)	32.2 (65.3)	27.1 (71.6)	159.2 (160.1)	160.2 (165.4)	151.6 (165.2)

based on a CRM with a stiffness equal or at the most twice of the dentin's and equipped with multiple glass-fibre reinforcements.

Acknowledgements

This work was developed within the framework of Lagrange Laboratory, a European research group comprising CNRS, CNR, the Universities of Rome 'Tor Vergata', Calabria, Cassino, Pavia and Salerno, Ecole Polytechnique, University of Montpellier II, ENPC, LCPC and ENTPE.

The cooperation of Riccardo Cottone and Michele Marino, graduate students at the School of Engineering, University of Rome 'Tor Vergata', offered for partial credit toward their Bachelor of Medical Engineering degrees, is gratefully acknowledged.

References

Anderson DJ. 1956. Measurement of stress in mastication. II. J Dent Res. 35:671–673.

Asmussen E, Peutzefeldt A, Heitmann T. 1999. Stiffness, elastic limit and strength of newer types of endodontic posts. J Dent. 27(4):275–278.

Asmussen E, Peutzfeldt A, Sahafi A. 2005. Finite element analysis of stresses in endodontically treated, dowel-restored teeth. J Prosthet Dent. 94(4):321–329.

Baraban DJ. 1967. The restoration of pulpless teeth. Dent Clin North Am. 11:633–653.

Barink M, Van der Mark PCP, Fennis WMM, Kuijs RH, Kreulen CM, Verdonschot N. 2003. A three-dimensional finite element model of the polymerization process in dental restorations. Biomaterials. 24(8):1427–1435.

Bisegna, P, Lagache, T, Maceri, F, Martignoni, M, Vairo, G. 2003. 17–18 July Three-dimensional finite element analysis of an endodontic restoration with fibre-reinforced multiple posts. Paper presented at the 10th FEM Workshop on Biomechanics and related fields, Ulm, Germany.

Brännström M. 1984. Communication between the oral cavity and the dental pulp associated with restorative treatment. Operat Dent. 9:57–68.

Craig RG. 1989. Restorative dental materials. St Louis: CV Mosby.

Davidson CL, Feilzer AJ. 1997. Polymerization shrinkage and polymerization shrinkage stress in polymer-based restorations. J Dent. 25:435–440.

Davidson CL, de Gee AJ. 1984. Relaxation of polymerization shrinkage stresses by flow in dental composites. J Dent Res. 63:146–148.

De Gee AJ, Feilzer AJ, Davidson CL. 1993. True linear polymerization shrinkage of unfilled resins and composites determined with a linometer. Dent Mater. 9:11–14.

Drucker DC. 1967. Introduction to the mechanics of deformable solids. New York: Mc-Graw Hill.

Eick JD, Welch FH. 1986. Polymerization shrinkage of posterior composite resins and its possible influence on postoperative sensitivity. Quintessence Int. 17:103–111.

Farah JW, Craig RG, Sikarskie DC. 1973. Photoelastic and finite element stress analysis of a restored axisymmetric first molar. J Biomech. 6:511–520.

Fernandes AS, Shetty S, Coutinho I. 2003. Factors determining post selection: a literature review. J Prosthet Dent. 90: 556–562.

Freedman G. 1996. The carbon fibre post: metal-free, post-endodontic rehabilitation. Oral Health. 86(2):29–30.

Genovese K, Lamberti L, Pappalettere C. 2005. Finite element analysis of a new customised composite post system for endodontically treated teeth. J Biomech. 38:2375–2389.

Goel VK, Khera SC, Gurusami S, Chen RCS. 1992. Effect of cavity depth on stresses on a restored tooth. J Prosthet Dent. 67:174–183.

Holmes DC, Diaz-Arnold AM, Leary JM. 1996. Influence of post dimension on stress distribution in dentin. J Prosthet Dent. 75:140–147.

Howell AH, Manly RS. 1948. An electronic strain gage for measuring oral forces. J Dent Res. 27:705–712.

Ho MH, Lee SY, Chen H, Lee MC. 1994. Three-dimensional finite element analysis of the effects of posts on stress distribution in dentin. J Prosthet Dent. 72:367–372.

Hübsch PF, Middleton J, Knox J. 2000. A finite element analysis of the stress at the restoration-tooth interface, comparing inlays and bulk fillings. Biomaterials. 21(10): 1015–1019.

Hübsch P, Middleton J, Knox J. 2002. The influence of cavity shape on the stresses in composite dental restorations: a finite element study. Comput Methods Biomech Biomed Eng. 5(5):343–349.

Ichim I, Kuzmanovic DV, Love RM. 2006. A finite element analysis of ferrule design on restoration resistance and distribution of stress within a root. Int Endod J. 39(6): 443–452.

Joshi S, Mukherjee A, Kheur M, Metha A. 2001. Mechanical performance of endodontically treated teeth. Finite Elem Anal Des. 37:587–601.

Kahn FH, Rosenberg PA, Schulman A, Pines M. 1996. Comparison of fatigue for three prefabricated threaded post systems. J Prosthet Dent. 75:148–153.

Karna JC. 1996. A fiber composite laminate endodontic post and core. Am J Dentist. 9(5):230–232.

Kleverlaan CJ, Feilzer AJ. 2005. Polymerization shrinkage and contraction stress of dental resin composites. Dent Mater. 21:1150–1157.

Ko C, Chu C, Chung K, Lee M. 1992. Effects of posts on dentine stress distribution in pulpless teeth. J Prosthet Dent. 68: 421–427.

Labella R, Lambrechts P, Van Meerbeek B, Vanherle G. 1999. Polymerization shrinkage and elasticity of flowable composites and filled adhesives. Dent Mater. 15:128–137.

Lanza A, Aversa R, Rengo S, Apicella D, Apicella A. 2005. 3D FEA of cemented steel, glass and carbon posts in a maxillary incisor. Dent Mater. 21:709–715.

Lee SY, Chiang HC, Lin CT, Huang HM, Dong DR. 2000. Finite element analysis of thermo-debonding mechanisms in dental composites. Biomaterials. 21(13):1315–1326.

Lee SY, Chiang HC, Huang HM, Shih YH, Chen HC, Dong DR, Lin CT. 2001. Thermo-debonding mechanisms in dentin bonding systems using finite element analysis. Biomaterials. 22(2):113–123.

Maceri, F, Martignoni, M, Vairo, G. 2007. Mechanical behaviour of endodontic restorations with multiple prefabricated posts: a finite element approach. J Biomech. 40:2386–2398.

Martinez-Insua A, da Silva L, Rilo B, Santana U. 1998. Comparison of the fracture resistances of pulpless teeth restored with a cast post and core or carbon-fiber post with a composite core. J Prosthet Dent. 80:527–532.

Nishigawa K, Bando E, Nakano M. 2001. Quantitative study of bite force during sleep associated bruxism. J Oral Rehabil. 28:485–491.

Nishihira M, Yamamoto K, Sato Y, Ishikawa H, Natali AN. 2003. Mechanics of periodonatal ligament. In: Natali AN, editor. Dental biomechanics. London: Taylor & Francis. p. 20–34.

Pegoretti A, Fambri L, Zappini G, Bianchetti M. 2002. Finite element analysis of a glass fiber reinforced composite endodontic post. Biomaterials. 23:2667–2682.

Pierrisnard L, Bohin F, Renault P, Barquins M. 2002. Corono-radicular reconstruction of pulpless teeth: a mechanical study using finite element analysis. J Prosthet Dent. 88(4): 442–448.

Romeed SA, Fok SL, Wilson NHF. 2006. A comparison of 2D and 3D finite element analysis of a restored tooth. J Oral Rehabil. 33:209–215.

Sidoli GE, King PA, Setchell DJ. 1997. An *in vitro* evaluation of a carbon fiber-based and core system. J Prosthet Dent. 78(1):5–9.

Silver-Thorn MB, Joyce TP. 1999. Finite element analysis of anterior tooth root stresses developed during endodontic treatment. J Biomech Eng. 121:108–115.

Toms SR, Dakin GJ, Lemons JE, Eberhardt AW. 2002. Quasi-linear viscoelastic behavior of the human periodontal ligament. J Biomech. 35:1411–1415.

Toparli M. 2003. Stress analysis in a post-restored tooth utilizing the finite element method. J Oral Rehabil. 30: 470–476.

Ukon S, Moroi H, Okimoto K, Fujita M, Ishikawa M, Terada Y, Satoh H. 2000. Influence of different elastic moduli of dowel and core on stress distribution in root. Dent Mater. 19: 50–64.

Vairo, G. 2003. 23–24 November Modellazione geometrica di interventi odontoiatrici per la simulazione del comportamento meccanico di denti curati (in Italian). Paper presented at the National Meeting of Italian Society for Computer Simulation ISCS, Cefalù, Italy.

Versluis A, Tantbirojn D, Pintado MR, DeLong R, Douglas WH. 2004. Residual shrinkage stress distributions in molars after composite restoration. Dent Mater. 20:554–564.

Yaman SD, Alacam T, Yaman Y. 1998. Analysis of stress distribution in a maxillar central incisor subjected to various post and core applications. J Endod. 24:107–111.

Zienkiewicz OC, Taylor RL. 1998. The finite element method. 4th ed. London: Mc-Graw Hill.